Vegetation response to climate zone dynamics and its impacts on surface soil water content and albedo in China

Guan, Yanlong

2020-12-10

Guan , Y , Lu , H , Yin , C , Xue , Y , Jiang , Y , Kang , Y , He , L & Heiskanen , J 2020 , '
Vegetation response to climate zone dynamics and its impacts on surface soil water content
and albedo in China ' , The Science of the Total Environment , vol. 747 , 141537 . https://doi.org/10.1016/j.scitotenv.2

http://hdl.handle.net/10138/332838
https://doi.org/10.1016/j.scitotenv.2020.141537

acceptedVersion

Vegetation response to climate zone dynamics and its impacts on surface soil water content and albedo in China

Yanlong Guan[1,2,4], Hongwei Lu[1,2*], Chuang Yin[2], Yuxuan Xue[1], Yelin Jiang[6], Yu Kang[2,1], Li He[3,2], Janne Heiskanen[4,5]

[1] Key Laboratory of Water Cycle and Related Land Surface Process, Institute of Geographic Science and Natural Resources Research, Chinese Academy of Science, Beijing, China

[2] School of Renewable Energy, North China Electric Power University, Beijing, China

[3] State Key Laboratory of Hydraulic Engineering Simulation and Safety at Tianjin University, Tianjin, China

[4] Department of Geosciences and Geography, University of Helsinki, Finland

[5] Institute for Atmospheric and Earth System Research, Faculty of Science, University of Helsinki, Finland

[6] Department of Civil and Environmental Engineering, University of Connecticut, Storrs, CT, USA

Corresponding author: Hongwei Lu (luhw@igsnrr.ac.cn)

Abstract

Extensive research has focused on the response of vegetation to climate change, including potential mechanisms and resulting impacts. Although many studies have explored the relationship between vegetation and climate change in China, research on spatiotemporal distribution changes of climate regimes using natural vegetation as an indicator is still lacking. Further, limited information is available on the response of vegetation to shifts in China's regional climatic zones. In this study, we applied Mann–Kendall, and correlation analysis to examine the variabilities in temperature, precipitation, surface soil water, normalised difference vegetation index (NDVI), and albedo in China from 1982 to 2012. Our results indicate significant shifts in the distribution of Köppen–Geiger climate classes in China from 12.08% to 18.98% between 1983 and 2012 at a significance level of 0.05 (MK). The percentage areas in the arid and continental zones expanded at a rate of 0.004%/y and 0.12%/y, respectively, while the percentage area in the temperate and alpine zones decreased by -0.05%/y and -0.07%/y. Sensitivity fitting results between simulated and observed changes identified temperature to be a dominant control on the dynamics of temperate (r^2=0.98) and alpine (r^2=0.968) zones, while precipitation was the dominant control on the changes of arid (r^2=0.856) and continental (r^2=0.815) zones. The response of the NDVI to albedo infers a more pronounced radiative response in temperate (r = –0.82, p < 0.01) and alpine (r = –0.476, p < 0.05) compared to arid and continental zones. Furthermore, we identified more pronounced monthly increasing trends in

NDVI and soil water, corresponding to weak changes in albedo during vegetation growing periods. Our results suggest that climate zone shifting has considerable impacts on the vegetation in China and will have larger ecological impacts through radiative or non-radiative feedback mechanisms in future warming scenarios.

Key words: Climate zones; Temperature; Precipitation; NDVI; Albedo

1 Introduction

Research work (Carey et al., 2017; Fan and van den Dool, 2008; Shen et al., 2015; Turco et al., 2017) has demonstrated that shifts in the climate system increase the likelihood of widespread and irreversible impacts on global ecosystems, including changes to vegetation greening/coverage (Abera et al., 2019; Erb et al., 2017; Fang et al., 2004; Harris et al., 2016; Helmens et al., 2018; Huang et al., 2016; Li et al., 2018; Piao et al., 2015; Richardson et al., 2013; Shen et al., 2015; Yang et al., 2018; Zhao, 2018). Vegetation supplies the materials and energy required to sustain life on Earth through photosynthesis by converting water and carbon dioxide to oxygen and carbohydrates. The length of the growing season and vegetation productivity are highly sensitive to changes in climate (Erasmi et al., 2017; Martin-Benito and Pederson, 2015; Turco et al., 2017). Greening and browning are measured by the NDVI changes, which are commonly correlated to vegetation productivity and biomass. These vegetation changes can alter the regional energy, carbon, and water balance, resulting in atmospheric warming or cooling, depending on the relative

impacts of radiative (albedo) and non-radiative processes (such as evapotranspiration and surface roughness length) (Abera et al., 2019; Li et al., 2015).

Many studies have explored the response mechanisms between climate change and vegetation processes at different scales. For example, in the context of global warming, increased vegetation productivity in the Arctic was shown to reduce surface albedo, resulting in positive temperature feedback (Pearson et al., 2013; Pithan and Mauritsen, 2014). Conversely, analysis of NDVI and evapotranspiration in the Tibetan Plateau inferred reduced surface warming in the growing season in response to increased vegetation activity (Shen et al., 2015). Gottfried et al. (2012) and Pauli et al. (2012) identified a link between ongoing continent-scale climate change and changing mountain plant communities, with a particular increase in the number of warm-adapted species due to thermophilization. Wu et al. (2015) applied NDVI and climatic data to demonstrate that the time-lag effect between vegetation and primary climate factors influences vegetation growth on a global scale.

The Köppen–Geiger classification (Peel et al., 2007; Rubel & Kottek, 2010) is often used to describe highly heterogeneous climate zones with different climatic conditions. It is one of the most widely accepted climate classification systems used to describe vegetation distribution based solely on annual and monthly temperature and precipitation patterns. The Köppen–Geiger criteria has been validated by a number of studies through its strong links between climate and biome type (Engelbrecht and Engelbrecht, 2016; Farmer and Cook, 2013; Rohli et al., 2015a), suggesting that its

dynamic characteristics still have significant research value in many fields of research today. This connection between climate and biomes provides the possibility of assessing the relationship between the empirical climate and natural vegetation (Guan et al., 2020; Guetter and Kutzbach, 1990).

Considering the nature of the climate classification, the change in vegetation response to climate should be presented simply and clearly. Garcia et al. (2014) reported that changes in the regional distribution of climate can affect the availability and distribution of climatically suitable areas for vegetation. The changes in specific climate zones suitable for the vegetation types are likely to result in the expansion or reduction of the distribution range of specific vegetation types. Rohli et al. (2015a) identified that the boundaries of the Köppen classes strongly overlapped with many ecological factors, such as vegetation distribution. Williams et al. (2007) suggested that novel and disappearing climates can lead to the disaggregation of vegetation species assemblages. Wang and Overland, (2004) reported a decline in the Arctic Tundra climate zone since the 1990s, accompanied by a marked increase in boreal and temperate groups. According to modelling results by Pearson et al. (2013), at least half of the Arctic vegetation coverage is expected to shift by 2050, with woody vegetation coverage expected to increase by 52% in response to specific climate change. In some areas where the tundra is replaced by shrubs, the albedo in the growing season will decrease.

Recent studies have shown that we can hypothesise that if shifts between climate zones occur constantly, vegetation will substantially respond to shifting climate zones and surface biophysical characteristics will change. Similar to changes in land cover, shifts in heterogeneous climate zones are highly likely to affect vegetation structure (e.g., canopy height), phenology, the seasonality of albedo, and even vegetation type succession, which in turn directly affect regional surface energy balance and net radiation partitioning (Richardson et al., 2013). However, the impacts of shifting climate zones on vegetation have not yet been fully addressed in China. In this regard, the combination of NDVI, soil water, and albedo variables can be effectively used to shed light on the impact of shifting climate zones on vegetation, further its surface biophysical characteristics. Thus, further examination using relatively high-resolution remote sensing observations and reanalysis data sets is needed, in the area that have undergone climate type shifts, to better understand the impact of temperature and precipitation to specific climate zones, and to clarify the potential response of vegetation to specific climate zones.

This study aims to determine the dynamic response of regional vegetation in China to the shifting climatic regimes and its resulting impact on surface biophysical characteristics from 1982 to 2012. In particular, we explored (1) the temporal shifts of the Köppen climate regions, including total climate zones, and specific arid, temperate, continental, and alpine climate regions; (2) the dominant drivers (temperature or precipitation) of the dynamics of specific climate zones; and (3) the

response of vegetation to changes in the four climate zones and its influence on surface soil water (SW) content and albedo. The exploration between vegetation response and the climate types involved can better estimate the uniqueness of climate change at a given scale, and may also inform our understanding of impacts of climate change on biome.

2 Study area

China’s climate is complex and diverse and is predominantly controlled by the distribution of temperature (Figure 1a), precipitation (Figure 1b), and topography (Figure 1c). The spatial distribution of temperature is primarily influenced by latitude and altitude (e.g., from Qinghai to the Tibetan Plateau) and ranges from −12.4. to 25.07 °C. The total precipitation gradually decreases from a maximum of 1937.5 mm in the southeast to a minimum of 8.3 mm in the northwest. During the warm season, the southern and eastern regions of China experience high rainfall due to the influence of the monsoon. In contrast, Northwest China experiences low precipitation due to its distance from the ocean. During the cold seasons, continental circulation causes most regions, particularly in the north and west, to be cold and dry. In general, China’s climate is geographically distinct and seasonally variable.

Given that climate is an important limiting factor in ecological processes, China's large spatial climate variability promotes the heterogeneous distribution of vegetation types and ecosystems (Figure 1d). China has a variety of land vegetation types,

including shrubs, swamps, broadleaf forests, meadows, coniferous forests, cultivated vegetation, alpine vegetation, grasslands, mixed forests, and deserts. From individual forms to spatial community distributions, vegetation is dependent on the temporal and spatial distribution of regional hydrothermal conditions.

Place Figure 1

---

3 Data and methods

3.1 Observed and reanalysis data

We utilised satellite-based vegetation data, climatic observational grid data, and reanalysis data from 1982 to 2012, including NDVI, temperature, precipitation, albedo, and surface volumetric SW (Table 1). To achieve a consistent spatial resolution for the analysis, we applied the bilinear method to interpolate the remote sensing and reanalysis data to regular 0.125° × 0.125° grids. To further reduce the impact of natural variability, a 5-year running mean was applied to all datasets to mitigate possible short-term variations (Mahlstein et al., 2013).

NDVI is an effective measurement of the photosynthetically active radiation absorbed by chlorophyll in the green leaves of vegetation canopies (Pinzon & Tucker, 2014).

Absorption in the visible spectral region and reflectance in the near infra-red region increases with increasing chlorophyll content, leaf area index (LAI), and healthy leaf structure, and thus greener and denser vegetation will result in relatively high NDVI (approaching one). We used the GIMSS NDVI3g (v0) dataset generated from the National Oceanic and Atmospheric Administration Advanced Very High Resolution Radiometer (AVHRR) (Tucker et al., 2005; Pinzon & Tucker, 2014). The data range from July 1982 to December 2011, has a resolution of 0.0833° and is carefully harmonised from different AVHRR sensors. Negative influences, such as calibration loss, volcanic eruptions, and orbital drift, were considered in data processing.

Albedo and volumetric soil water (SW) reanalysis data were obtained from the European Centre for Medium-Range Weather Forecasts. The reanalysis data were produced by combining weather forecast models with observations using data assimilation, that is, the four-dimensional variational assimilation (4D-Var) method (Dee et al., 2011). In general, this is an incremental and iterative method to minimise a cost function to reduce the biases between observed values and the available short-range forecasts (Flemming et al., 2015). These datasets have been produced and archived on a reduced Gaussian grid, which has quasi-uniform spacing across the globe. Specifically, reduced Gaussian grids have a series of evenly spaced data grids along each latitude, which are spaced at quasi-regular intervals. Close to the equator, there are many points along a latitude parallel, but near the pole, only a few points along a latitude parallel. Furthermore, the datasets were interpolated to a regular grid

at a horizontal resolution of 0.125°. The default interpolation method is bilinear for our continuous parameters (e.g., albedo and SW). For SW data, we used the surface layer at a range of 0–7 cm, as surface soil moisture affected by temperature and precipitation is sensitive to vegetation change (McColl et al., 2017). For albedo data, in the short-wave radiation scheme, the surface reflection is handled by combining direct and diffuse radiation. Over land, surface albedo is derived from the monthly mean climatology of its visible and near-infrared direct and diffuse components built from MODIS albedo over the years 2000-2003 (Park, 2010; Schaaf et al., 2002). It can be used to assess potential environmental impacts from vegetation changes in different climatic regions, such as impacts on the regional energy balance.

China's ground temperature and precipitation grid datasets (V2.0) at 0.5 ° × 0.5 ° resolution were provided by the National Meteorological Information Center of the China Meteorological Administration. The data cover most of China, excluding Taiwan, with 2472 national-level meteorological observation stations. Topography and vegetation type datasets were provided by the Geospatial Data Cloud (http://www.gscloud.cn/) and Resource and Environmental Data Clouds Platform from the Chinese Academy of Science (http://www.resdc.cn), respectively. These datasets have been widely applied in regional climate change research in China (Ren et al., 2015), and they provided accurate data for mapping the spatial distribution of Köppen–Geiger climatic types in the present study. We also collected monthly gridded precipitation and temperature datasets at 0.5 ° × 0.5 ° resolution from the

University of East Anglia Climatic Research Unit (CRU TS V.4.02) (Harris et al., 2014) to generate the Köppen map. CRU TS V.4.02 provides a gridded time-series dataset based on observations from more than 4,000 sites over land.

Place Table 1

3.2 Köppen–Geiger climate classification

We used the Köppen–Geiger climate classification (Peel et al., 2007) to divide China into five climatic categories: tropical (A), arid (B), temperate (C), continental (D), and alpine (E) (Table S1). Given that the annual shifts in these climate zones may produce unrelated trends in the calculated results prior to the climate zoning analysis, we first applied the 5-year running mean to eliminate biases in climate variability (Mahlstein et al., 2013). Then, we determined the cumulative percentage of area change of all climatic zones during 1982–2012 relative to the spatial distribution in the first year (1982) (Huang et al., 2020). As each grid was assigned an initial climate category, altered grids were included if they shifted to a new climate type. Percentage area of specific climate was based on the number of grids of different climate types. To validate the applicability of our results, we compared the maps over the period 1982–

2012 to the map generated by the Climatic Research Unit (CRU) monthly temperature and precipitation (Figure S1-2).

3.3 Statistical analysis

One of the widely used non-parametric trend tests is the Mann–Kendall trend test (Text S1) (Mann, 1945; Kendall, 1975), which has been widely used to assess the significance of trends in meteorological time series. The null hypothesis in the Mann-Kendall test is that the data are independent and randomly ordered. The results elucidate the magnitude of the correlation and the direction of the relationship. The value of the coefficient ranges from 1 to –1, indicating a positive correlation and a negative correlation, respectively. Furthermore, we assume that the data are normally distributed. The null hypothesis states that the population correlation coefficient is equal to zero, which indicates that there is no linear correlation between the environmental variables. An alternative hypothesis was that it is not equal to zero. The t-test was used to determine whether the correlation coefficient was significantly different from zero, indicating an association between the two variables.

3.4 Sensitivity analysis

We conducted a sensitivity analysis to evaluate the evolution of climate zones in response to temperature and precipitation. First, we separately maintained each monthly temperature or precipitation at the same value as the initial year (1982) to compute the simulated percentage area of each climate zone. Second, we compared the experimental results with the observed percentage area of each zone to identify the

relative influence of the two climatic factors (e.g., either temperature or precipitation). Lastly, we utilised the coefficient of determination (r^2) and significance (p) value to determine the sensitivity of each climate zone to temperature and precipitation.

4 Results

4.1 Spatiotemporal variability of temperature, precipitation, and vegetation

We observed that the linear trends of annual temperature and precipitation featured clear spatial characteristics during 1982–2012 (Figure 2a-b). The highest rates of temperature rise were located in the Qinghai–Tibet Plateau (0.07 °C/y), East Inner Mongolia (0.05 °C/y), and the lower reaches of the Yangtze River (0.05 °C/y), while negative trends were most prominent in Northeast China (-0.01 °C/y). Negative trends in precipitation were predominantly observed in the middle and lower reaches of the Yangtze River (-25.2 mm/y), the Yunnan–Guizhou Plateau (-17.2 mm/y), and the Northeast Plain (-15.3 mm/y). Meanwhile, large increases in precipitation were observed in Northwest China, such as the Tianshan mountain region (6.3 mm/y) and the Qinghai–Tibet Plateau (9.4 mm/y).

In addition, we observed that the correlation between temperature and precipitation and NDVI between 1982 and 2012 has obvious regional characteristics. Overall, the temperature change ($p < 0.05$, MK) has a greater impact on vegetation growth than precipitation nationwide, especially in southern China and the Qinghai-Tibetan Plateau (Figure 2c), where NDVI is more sensitive to temperature changes. However,

NDVI in eastern Inner Mongolia and Tianshan area is more sensitive to precipitation decrease, with a significance level of 0.05 (t-test).

The spatiotemporal changes in temperature and precipitation will alter the regional climate zonation based on the Köppen–Geiger climate classification, and different climatic zones are likely to have varying sensitivities to the changes. For example, the rapid temperature increase in the Qinghai–Tibet Plateau is likely to result in a shrinking of the alpine climate zone and an expansion of the continental climate zone, triggering a rapid response to vegetation changes, including types and distribution. Furthermore, the observed decrease in precipitation in the Northeast Plain is likely to lead to the expansion of arid climate zones.

Place Figure 2

4.2 Spatiotemporal variability in the climate zone

Figure 3 illustrates the spatial distribution of China's climate zones in 1982, 1990, 2000, and 2010. Table 2 compares the 1990, 2000, and 2010 results relative to the baseline time (1982). The comparisons of 1982 to 1990 and 2000 to 2010 show that the percentage areas of arid zones are, respectively, reduced by -1.1% and -1.74%, but expanded from 1990 to 2000. In space, the largest changes in the percentage area of

arid zones were concentrated on the North China Plain and the Northeast Plains. Many areas alternated between the continental and arid climates—particularly in the northeast—in response to changes in precipitation, such as the marked precipitation reduction from 1990 to 2005 (Figure 2b). The percentage area of the temperate zone has expanded since 1982, with the highest increase (1.34%) observed from 1982 to 1990. Spatially, these changes occurred at the northern boundary of the temperate zone. The boundary between the Qinling Mountain and the Huaihe River Line shifted towards the north between 1982 and 1990, and gradually back towards the south thereafter. The temporal trends in the percentage area of the continental zone are directly opposite to the trend in the arid zone, which expanded by 0.2% and 1.95% from 1982 to 1990, and from 2000 to 2010, respectively, and reduced by -3.72% from 1990 to 2000. The total percentage area of the alpine zone has decreased consistently since 1982. Spatially, these changes occurred at the boundary between the alpine and continental zones. The areal expansion of the temperate zone resulted in the alpine zone in the Qinghai–Tibet Plateau shrinking, which has been predominantly replaced by the continental zone. In general, we observed clear fluctuations in the percentage area of arid, temperate, and continental zones, and a continued decrease in the percentage area of alpine zone since 1982.

Place Figure 3

300 ----------

301 ----------

302 **Place Table 2**

303 ----------

304 Figure 4 indicates that the cumulative percentage of area change in all climate zones
305 significantly increased from 12.08% to 18.98% at a rate of 0.204%/y from 1983 to
306 2012 at a significance level of 0.05 (MK). However, we observed differences in the
307 percentage area change between each climate zone from 1982 to 2012 (Figure 5). In
308 general, the arid and continental zones expanded at rates of 0.004%/y and 0.12%/y,
309 respectively, while the percentage areas of temperate and alpine zones decreased by -
310 0.05%/y and -0.07%/y at a significance level of 0.05, respectively. Moreover, we
311 detected a signal over each climate zone in 2005, where the percentage areas of the
312 arid and temperate zones evidently decreased from 34.46% to 25.26% and 22.8% to
313 22.52%, respectively. The area of the continental and alpine zones increased from
314 26.01% to 34.1% and 16.58% to 17.32%, respectively. These change trends around
315 2005 should be attributed to the differential response of specific climate zones to
316 notable changes in temperature and precipitation.

317 ----------

318 **Place Figure 4**

Place Figure 5

4.3 Climate zone sensitivity to driving forces

Figure 6 and Table 3 show the linear fitting results of the sensitivity experiments between observed and simulated percentage areas for specific climate zones in different scenarios during 1982–2012. Where temperature is held constant, the simulated change in the percentage area approximates the observed changes with r^2 of 0.855 and 0.815 ($p < 0.01$, t-test) in arid and continental zones, respectively. In this case, the linear fitting coefficients between the simulated and observed changes are 0.646 and 0.514 ($p < 0.01$, t-test) in the temperate and alpine zones, respectively. On the contrary, where precipitation is held constant, the linear fitting coefficients of simulated to observed changes are 0.473 and 0.753 ($p < 0.01$, t-test) in arid and continental zones, respectively. However, the correlation between the observed and simulated percentage area was stronger with temperature change, with r^2 values of 0.98 and 0.968 ($p < 0.01$, t-test) in the temperate and alpine zones, respectively. In general, through sensitivity analysis, precipitation seems to be the main driver in the dynamics of arid and continental zones, while temperature dominates the area change

of temperate and alpine zones. However, considering the nature of the Köppen scheme, temperature and precipitation essentially determine the changes in different climate zones. Therefore, we cannot ignore the important role of non-dominant factors in their respective climate zones. Particularly, in the continental zone the fitting coefficients between the simulated and observed changes in different scenarios are relatively close, with r^2 values of 0.815 and 0.753, respectively, indicating that temperature change also plays an important role in the change process in specific climate zone.

Place Figure 6

Place Table 3

---

352 4.4 Response of vegetation to climate zone and links to surface soil water content and
353 albedo

354 Figure 7 shows the trends in the annual SW content, NDVI, albedo, and the
355 correlation between albedo and NDVI for the period 1982–2012. Spatial changes in
356 NDVI are related to surface moisture and albedo. We observed a decrease in surface
357 SW content in the Northeast Mountains area and South China (Figure 7a). In contrast,
358 we observed a gradual increase in soil moisture content in the middle and west of
359 Tibet, the Northeast plain, and the Huaihe River Basin. We observed an increase in
360 NDVI in the Northeast Plain, Huaihe River Basin, and the Tianshan Mountains
361 (Figure 7b), and a decrease in NDVI in the Northeast, Yangtze River, Pearl River, and
362 Yunnan–Guizhou Plateau. The albedo trends of the middle and lower reaches of the
363 Yangtze River Basin, the Northeast Mountains, Southern China, and the Western
364 border mountains are more pronounced than elsewhere (Figure 7c). Figure 7d
365 illustrates the correlation between the NDVI and albedo. Albedo and NDVI were
366 positively correlated in Central and Western China, particularly in the Northeast plain,
367 the Yarlung Zangbo River Basin, and in Eastern Inner Mongolia.

368 ----------

369 **Place Figure 7**

370 ----------

Figure 8 depicts the relationship between the percentage area of each climate zone and their dominant driving factors (precipitation or temperature based on the sensitivity experiments), NDVI, and SW anomalies during 1982–2012. In general, changes in the percentage area of each climate zone are clearly related to the dominant driving factor, while changes in NDVI are influenced directly by SW content affected by the climate zone.

The percentage area of the arid zone increased slightly prior to 2005, which was consistent with changes in precipitation (Figure 8a). In contrast, the percentage area of arid zones decreased after 2005, which is opposite to the observed precipitation trend. With the rapid increase in precipitation, the percentage area of the arid zone and SW tended to decrease. Temperature was the dominant control on the percentage area of temperate zones. After 2005, the percentage area reduced from 27.91% to 26.52% in response to a temperature decrease from 16.71 °C to 16.16 °C. Since 2005, the area reduction of temperate climate has been concentrated on the North China Plain, where precipitation and SW have increased rapidly. Due to the decrease in coverage of temperate zones and the decrease in precipitation in the Yangtze River area, NDVI decreased from 0.646 to 0.524 since 2005. The percentage area of the continental zone increased from 23.36% to 27.20% in response to an increase in precipitation from 472 mm to 572 mm, as the evolution of the continental zone is more sensitive to changes in precipitation than changes in temperature. With the decrease in precipitation and SW before 2005, the disappearing area was mainly in the Northeast

Plain, and the overall NDVI of the continental zone increased due to the increase in the proportion of forest area. Since 2005, due to the rapid increase in precipitation, the percentage area has also increased rapidly, particularly in the Northeast Plain and Qinghai-Tibet Plateau, which decreased the overall SW and NDVI in the continental zone. The percentage area of the alpine zone was negatively correlated with changes in temperature and SW. Prior to 2005, the percentage area decreased from 21.9% to 20.9% in response to increasing temperature from –4.8 °C to –3.7 °C. However, the percentage area expanded from 20.9% to 21.2% and the NDVI increased from 0.371 to 0.379 since 2005 in response to a temperature change from –3.7 °C to –4.3 °C. Since 2005, the emerging area of the alpine zone has been concentrated between the alpine zone and the continental zone where the vegetation status is usually more productive than of that in the alpine zone.

Place Figure 8

Figure 9 shows the response of annual NDVI variability to albedo from 1982 to 2012. In general, there are evident differences between NDVI and albedo in different climate zones. For temperate and alpine climate zones, we found that the changes in NDVI were significantly correlated to albedo (p <0.05, t-test) during 1982–2012, in which the higher NDVI basically corresponds to lower albedo. However, the

412 relationship between albedo and NDVI is more complex in arid and continental
413 climates, particularly during 1995–2005.

414 The NDVI correlated significantly with albedo (r = –0.82, p < 0.01) in the temperate
415 zone (Figure 9b). Surface SW content after 2005 resulted in a rapid decrease of NDVI
416 from 0.32 to 0.28, while the albedo increased from 0.17 to 0.18. NDVI also correlated
417 significantly with albedo during 1982–2012 (r = –0.476, p < 0.05) in the alpine zone.
418 Changes in temperature and surface SW since 2005 resulted in an increase in NDVI
419 and a decrease in albedo from 0.187 to 0.185.

420 In the arid and continental climate zones, the NDVI variability during 1982–1995 and
421 2005–2012 was negatively correlated with albedo, while NDVI variability positively
422 correlated with albedo during the period 1995–2005. In particular, the observed
423 changes in 1995–2005 predominantly occurred in the Northeast Plain, where
424 precipitation had reduced and caused an increase in albedo. Precipitation is the
425 dominant control on the evolution of arid and continental climate zones, as changes in
426 precipitation caused notable shifts in the two climate types. Cultivated vegetation is
427 predominantly distributed in the Northeast Plain, according to the Chinese vegetation
428 atlas (2000). The NDVI increased from 1995 to 2005 in arid climate zones, as the
429 NDVI in the changed area was clearly higher than in low shrubland, meadows, and
430 desert regions. Furthermore, decreasing precipitation in continental climate zones had
431 reduced NDVI from 0.45. to 0.43, while albedo decreased from 0.183 to 0.181 from
432 1995 to 2005.

433 ----------

434 **Place Figure 9**

435 ----------

436 Figure 10 further highlights the observed differences in NDVI, albedo, and SW trends
437 of specific climate zones. SW content and NDVI predominantly increased and the
438 albedo decreased during the vegetation growing periods. The SW content in the arid
439 zone significantly decreased from February to April at rates of -0.4×10^{-3} m^3 m^{-3}/y to
440 -0.7×10^{-3} m^3 m^{-3}/y. We also observed significant decreases in February, March,
441 April, and September (continental zones). A significant increasing trend in June and a
442 decreasing trend in March and September were detected in the alpine climate zone.
443 The significant decrease in NDVI occurred in November and December during the
444 non-vegetation growing period (continental zones). Furthermore, in the arid and
445 alpine zones, the monthly trends of albedo increased, while predominant trends in
446 temperate and continental climates decreased. More importantly, weak changes in
447 albedo accompanied the strong trends in NDVI and SW content during the vegetation
448 growing periods.

449 ----------

450 **Place Figure 10**

451 ----------

5 Discussion

The spatial scales at which climate changes are measured are extremely important, since the response mechanism may change as the scale changes (Aalto et al., 2018; Chen et al., 2017; Järvi et al., 2019; Wu, 2004). On the one hand, our results reveal that major climate zones respond differently to changes in temperature and precipitation, indicating that arid and continental zones are more sensitive to precipitation, while temperate and alpine zones are more responsive to temperature. It should be noted that global universal climate change laws are not necessarily applicable to regional-scale climate change. Recent studies (Burrows et al., 2011; Lu et al., 2019; Mahlstein et al., 2013; Sunday et al., 2011) have shown that global warming determines the dynamics of global climate zones. However, our results demonstrate that it does not necessarily determine the dynamics in regional climate zones. On the other hand, we must consider the climate zone change at different spatial resolutions, as the statistical results may change as the possible uncertainty of different spatial resolutions. In this study, we selected regional high-density meteorological data with a resolution of 0.5° to explore changes in regional climate zones. This is because the application of relatively coarse spatial resolution may limit the effectiveness of climatic assessments and potential ecological impacts, particularly when it is insufficient to describe small-scale features such as in some high mountain areas (Beck et al., 2018; Rohli et al., 2015b). In view of this, climate change research

must fully consider the selection of a suitable spatial research scale and resolution because this will help us understand the climate itself (Guan et al., 2020).

In addition, our results demonstrate that overall changes in the percentage area of each climate zone were related to surface SW content, NDVI, and albedo in regions of high (temperate zones) and low (alpine zones) vegetation coverage. Since climate zones are considered a substitute for vegetation distribution (Rohli et al., 2015; Wang & Overland, 2004), regional climate zones may show some similarities in the surface biophysical properties of land cover. Changes in land cover influence radiative forcing and have been shown to directly affect regional energy balances (Abera et al., 2019a; Lee Et al., 2011; Li et al., 2015). Similar to shifts in land cover, when climate zones expand or shrink in response to changes in regional temperature or precipitation, these changes can also affect the greening or browning of regional vegetation (Chen et al., 2019), altering regional surface roughness, albedo, evaporation, and net radiation partitioning. However, it is not easy to fully elucidate the interactive mechanisms and feedbacks related to the regional energy balance based on shifts of climate zones, such as at the pixel level (Armstrong et al., 2016; Gerken et al., 2018; Stark et al., 2016). This is due to the lack of observational data on key climatic and biophysical variables, particularly in remote regions. Furthermore, according to the empirical nature of the Köppen classification scheme, the fluctuating climatic zone is significantly different from the surface reference for vegetation cover

with multi-year persistence. Despite these limitations, the study still effectively sheds light on the impact of shifting climate zones on the surface biophysical characteristics.

Our results also indicate inconsistencies in the correlations between climate zone shifts, NDVI and albedo in arid and continental climate zones. From 1995 to 2005, the precipitation-controlled shifts between arid and continental zones were mainly concentrated in the Northeast Plain. Due to the decrease in precipitation (Figure 2b), the continental zone in the Northeast Plain was replaced by arid zones. However, there was no obvious change in the type and distribution of vegetation, which may not only be due to human activities but also likely affected by the inertness of modern ecosystems to climate change (Scheffer et al., 2001). On the one hand, human activities such as large-scale agricultural reclamation and irrigation (Piao et al., 2003; Zhu et al., 2013) could change regional soil properties (e.g., moisture, pH, organic matter, nitrogen, and microorganisms) to affect the succession of vegetation types (Jiang et al., 2020), further influencing the biophysical characteristics of vegetation types. On the other hand, the threshold range of precipitation in response to different vegetation types could be more stable than that of the precipitation range of the Köppen arid climate (Mahlstein et al., 2013; Peel et al., 2007). Zhao et al. (2015) indicated that a threshold effect may exist in the vegetation response to climate change in many ecosystems. Although it is difficult to distinguish the different effects quantitatively, internal and external feedback jointly promote the stability of regional ecosystems and vegetation types.

6 Conclusion

In this study, we investigated the vegetation response to shifting climate zones and its potential impacts on albedo and SW content in China. As the substantial changes in temperature and precipitation across time and space, we detected significant shifts in climate zonation on a nationwide level. From 1983 to 2012, the cumulative percentage of area change in all climate zones significantly increased from 12.08% to 18.98% at an annual growth rate of 0.204% ($p < 0.05$, MK). The percentage areas of arid and continental zones expanded at rates of 0.004%/y and 0.12%/y, respectively, while the temperate and alpine zones decreased by -0.05%/y and -0.07%/y, respectively. Sensitivity results in the different simulated cases suggest that the temperature and precipitation impact in specific climate zones are different. Specifically, temperature is the dominant control on the evolution of temperate and alpine zones with r^2 of 0.98 and 0.968 between simulated and observed changes, respectively, while precipitation is the dominant control on the evolution of arid and continental zones with r^2 of 0.856 and 0.815, respectively. Vegetation substantially responds to shifting climate zones with impact on surface biophysical characteristics. Specifically, a pronounced albedo and NDVI feedback response was detected in temperate and alpine zones with a 0.05 significance level. However, inconsistent feedbacks of NDVI to albedo were also reported in arid and continental climates, particularly during 1995-2005. Furthermore, recent climate warming has influenced

the seasonal trends in vegetation activity. The SW content and NDVI predominantly increased and the albedo decreased during the vegetation growing periods.

In general, the redistribution of vegetation has emerged as one of the most pronounced biological responses to climate change. Considering that the vegetation distribution represents an expression of 'visible climate', the rapid increase or decrease of climate-suitable areas will alter their distributional ranges and seasonal activities to maintain their niche, especially as the global temperature may increase by at least 1.5°C in the near future. If the speed of vegetation species tracks or adaptions to climate conditions cannot reach the rate of climate change, it may lead to the disaggregation of vegetation species assemblages, and the spatial distribution of original vegetation will be gradually replaced by novelty vegetation, in which regional surface biophysical characteristics and radiative mechanisms will inevitably change, especially in the event of accelerated warming in the future. Moreover, future relevant analysis may be useful in a wide range of environmental topics, especially with the advent of continuous high-quality and high-resolution data products, which will improve our ability to describe climate types in areas of sharp climatic gradients (e.g. mountainous areas of the Qinghai-Tibet Plateau).

Acknowledgments

We appreciate National Meteorological Information Center (NMIC) of the China and the Global Inventory Monitoring and Modeling System (GIMMS) project as well as

European Centre for Medium-Range Weather Forecasts (ECMWF) to provide the public observed and reanalyzed datasets. This research is supported by the Strategic Priority Research Program of Chinese Academy of Sciences (XDA20040301), the National Natural Science Foundation of China (41890824), and the Fundamental Research Funds for the Central Universities. The data archiving in this study has archived at the Mendeley repository (https://data.mendeley.com/). Furthermore, we would like to thank anonymous reviewers for their useful comments on the manuscript.

Reference:

Aalto, J., Karjalainen, O., Hjort, J., Luoto, M., 2018. Statistical Forecasting of Current and Future Circum-Arctic Ground Temperatures and Active Layer Thickness. Geophys. Res. Lett. 45, 4889–4898. https://doi.org/10.1029/2018GL078007

Abera, T.A., Heiskanen, J., Pellikka, P., Rautiainen, M., Maeda, E.E., 2019. Clarifying the role of radiative mechanisms in the spatio-temporal changes of land surface temperature across the Horn of Africa. Remote Sens. Environ. 221, 210–224. https://doi.org/10.1016/j.rse.2018.11.024

Armstrong, E., Valdes, P., House, J., Singarayer, J., 2016. The role of CO2 and dynamic vegetation on the impact of temperate land-use change in the HadCM3 coupled climate model. Earth Interact. 20. https://doi.org/10.1175/EI-D-15-0036.1

574 Beck, H.E., Zimmermann, N.E., McVicar, T.R., Vergopolan, N., Berg, A., Wood,
575 E.F., 2018. Present and future köppen-geiger climate classification maps at 1-km
576 resolution. Sci. Data 5, 1–12. https://doi.org/10.1038/sdata.2018.214
577 Burrows, M.T., Schoeman, D.S., Buckley, L.B., Moore, P., Poloczanska, E.S.,
578 Brander, K.M., Brown, C., Bruno, J.F., Duarte, C.M., Halpern, B.S., Holding, J.,
579 Kappel, C. V., Kiessling, W., O'Connor, M.I., Pandolfi, J.M., Parmesan, C.,
580 Schwing, F.B., Sydeman, W.J., Richardson, A.J., 2011. The pace of shifting
581 climate in marine and terrestrial ecosystems. Science (80-.). 334, 652–655.
582 https://doi.org/10.1126/science.1210288
583 Carey, M., Molden, O.C., Rasmussen, M.B., Jackson, M., Nolin, A.W., Mark, B.G.,
584 2017. Impacts of Glacier Recession and Declining Meltwater on Mountain
585 Societies. Ann. Am. Assoc. Geogr. 107, 350–359.
586 https://doi.org/10.1080/24694452.2016.1243039
587 Chen, C., Park, T., Wang, X., Piao, S., Xu, B., Chaturvedi, R.K., Fuchs, R., Brovkin,
588 V., Ciais, P., Fensholt, R., Tømmervik, H., Bala, G., Zhu, Z., Nemani, R.R.,
589 Myneni, R.B., 2019. China and India lead in greening of the world through land-
590 use management. Nat. Sustain. 2, 122–129. https://doi.org/10.1038/s41893-019-
591 0220-7
592 Chen, T., Zhang, H., Chen, X., Hagan, D.F., Wang, G., Gao, Z., Shi, T., 2017. Robust
593 drying and wetting trends found in regions over China based on Köppen climate
594 classifications. J. Geophys. Res. 122, 4228–4237.
595 https://doi.org/10.1002/2016JD026168

596 Dee, D.P., Uppala, S.M., Simmons, A.J., Berrisford, P., Poli, P., Kobayashi, S.,
597 Andrae, U., Balmaseda, M.A., Balsamo, G., Bauer, P., Bechtold, P., Beljaars,
598 A.C.M., van de Berg, L., Bidlot, J., Bormann, N., Delsol, C., Dragani, R.,
599 Fuentes, M., Geer, A.J., Haimberger, L., Healy, S.B., Hersbach, H., Hólm, E. V.,
600 Isaksen, L., Kållberg, P., Köhler, M., Matricardi, M., Mcnally, A.P., Monge-
601 Sanz, B.M., Morcrette, J.J., Park, B.K., Peubey, C., de Rosnay, P., Tavolato, C.,
602 Thépaut, J.N., Vitart, F., 2011. The ERA-Interim reanalysis: Configuration and
603 performance of the data assimilation system. Q. J. R. Meteorol. Soc. 137, 553–
604 597. https://doi.org/10.1002/qj.828
605 Editorial Board for Chinese Vegetation Map, Chinese Academy of Sciences.
606 Vegetation Atlas of China (1:100000). Beijing: Science Press, 2001: 129-132.
607 Engelbrecht, C.J., Engelbrecht, F.A., 2016. Shifts in Köppen-Geiger climate zones
608 over southern Africa in relation to key global temperature goals. Theor. Appl.
609 Climatol. 123, 247–261. https://doi.org/10.1007/s00704-014-1354-1
610 Erasmi, S., Dulamsuren, C., Hauck, M., Klinge, M., Karger, D.N., 2017. Climate
611 effects on the vitality of boreal forests at the treeline in different ecozones of
612 Mongolia. Biogeosciences Discuss. 1–25. https://doi.org/10.5194/bg-2017-220
613 Erb, K.H., Luyssaert, S., Meyfroidt, P., Pongratz, J., Don, A., Kloster, S., Kuemmerle,
614 T., Fetzel, T., Fuchs, R., Herold, M., Haberl, H., Jones, C.D., Marín-Spiotta, E.,
615 McCallum, I., Robertson, E., Seufert, V., Fritz, S., Valade, A., Wiltshire, A.,
616 Dolman, A.J., 2017. Land management: data availability and process
617 understanding for global change studies, Global Change Biology.

https://doi.org/10.3945/ajcn.116.130518

Fan, Y., van den Dool, H., 2008. A global monthly land surface air temperature analysis for 1948-present. J. Geophys. Res. Atmos. 113, 1–18. https://doi.org/10.1029/2007JD008470

Fang, J., Piao, S., He, J., Ma, W., 2004. Increasing terrestrial vegetation activity in China, 1982-1999. Sci. China, Ser. C Life Sci. 47, 229–240. https://doi.org/10.1360/03yc0068

Farmer, G.T., Cook, J., 2013. Climate change science: A modern synthesis: Volume 1 - The physical climate. Clim. Chang. Sci. A Mod. Synth. Vol. 1 - Phys. Clim. 1, 1–564. https://doi.org/10.1007/978-94-007-5757-8

Flemming, J., Huijnen, V., Arteta, J., Bechtold, P., Beljaars, A., Blechschmidt, A.M., Diamantakis, M., Engelen, R.J., Gaudel, A., Inness, A., Jones, L., Josse, B., Katragkou, E., Marecal, V., Peuch, V.H., Richter, A., Schultz, M.G., Stein, O., Tsikerdekis, A., 2015. Tropospheric chemistry in the integrated forecasting system of ECMWF. Geosci. Model Dev. 8, 975–1003. https://doi.org/10.5194/gmd-8-975-2015

Garcia, R.A., Cabeza, M., Rahbek, C., Araújo, M.B., 2014. Multiple dimensions of climate change and their implications for biodiversity. Science (80-.). 344. https://doi.org/10.1126/science.1247579

Gerken, T., Ruddell, B.L., Fuentes, J.D., Araújo, A., Brunsell, N.A., Maia, J., Manzi, A., Mercer, J., dos Santos, R.N., von Randow, C., Stoy, P.C., 2018. Investigating the mechanisms responsible for the lack of surface energy balance closure in a

640 central Amazonian tropical rainforest. Agric. For. Meteorol. 255, 92–103.
641 https://doi.org/10.1016/j.agrformet.2017.03.023
642 Gottfried, M., Pauli, H., Futschik, A., Akhalkatsi, M., Barančok, P., Benito Alonso,
643 J.L., Coldea, G., Dick, J., Erschbamer, B., Fernández Calzado, M.R., Kazakis,
644 G., Krajči, J., Larsson, P., Mallaun, M., Michelsen, O., Moiseev, D., Moiseev, P.,
645 Molau, U., Merzouki, A., Nagy, L., Nakhutsrishvili, G., Pedersen, B., Pelino, G.,
646 Puscas, M., Rossi, G., Stanisci, A., Theurillat, J.-P., Tomaselli, M., Villar, L.,
647 Vittoz, P., Vogiatzakis, I., Grabherr, G., 2012. Continent-wide response of
648 mountain vegetation to climate change. Nat. Clim. Chang. 2, 111–115.
649 https://doi.org/10.1038/nclimate1329
650 Guan, Y., Lu, H., He, L., Adhikari, H., Pellikka, P., Maeda, E., Heiskanen, J., 2020.
651 Intensification of the Dispersion of the Global Climatic Landscape and its
652 Potential as a New Climate Change Indicator. Environ. Res. Lett. 10, in press.
653 Guetter, P.J., Kutzbach, J.E., 1990. A modified Köppen classification applied to
654 model simulations of glacial and interglacial climates. Clim. Change 16, 193–
655 215. https://doi.org/10.1007/BF00134657
656 Harris, I., Jones, P.D., Osborn, T.J., Lister, D.H., 2014. Updated high-resolution grids
657 of monthly climatic observations - the CRU TS3.10 Dataset. Int. J. Climatol. 34,
658 623–642. https://doi.org/10.1002/joc.3711
659 Harris, R.M.B., Remenyi, T.A., Williamson, G.J., Bindoff, N.L., Bowman, D.M.J.S.,
660 2016. Climate–vegetation–fire interactions and feedbacks: trivial detail or major
661 barrier to projecting the future of the Earth system? Wiley Interdiscip. Rev.

662 Clim. Chang. 7, 910–931. https://doi.org/10.1002/wcc.428
663 Helmens, K.F., Katrantsiotis, C., Sakari Salonen, J., Shala, S., Bos, J.A.A., Engels, S.,
664 Kuosmanen, N., Luoto, T.P., Väliranta, M., Luoto, M., Ojala, A., Risberg, J.,
665 Weckström, J., 2018. Warm summers and rich biotic communities during N-
666 Hemisphere deglaciation. Glob. Planet. Change 167, 61–73.
667 https://doi.org/10.1016/j.gloplacha.2018.05.004
668 Huang, J., Yu, H., Guan, X., Wang, G., Guo, R., 2016. Accelerated dryland expansion
669 under climate change. Nat. Clim. Chang. 6, 166–171.
670 https://doi.org/10.1038/nclimate2837
671 Huang, X., Ma, L., Liu, T., Sun, B., Zhou, Y., Chen, Y., Qiao, Z., 2020. Spatial
672 Variability in Years of Abrupt Seasonal Temperature Changes and Warming
673 (Cooling) Hiatuses in China from 1951–2018 and the Variation Trends before
674 and after These Years. Atmosphere (Basel). 11, 82.
675 https://doi.org/10.3390/atmos11010082
676 Järvi, L., Havu, M., Ward, H.C., Bellucco, V., McFadden, J.P., Toivonen, T.,
677 Heikinheimo, V., Kolari, P., Riikonen, A., Grimmond, C.S.B., 2019. Spatial
678 Modeling of Local-Scale Biogenic and Anthropogenic Carbon Dioxide
679 Emissions in Helsinki. J. Geophys. Res. Atmos. 8363–8384.
680 https://doi.org/10.1029/2018jd029576
681 Jiang, Y., Guo, J., Peng, Q., Guan, Y., Zhang, Y., Zhang, R., 2020. The effects of
682 climate factors and human activities on net primary productivity in Xinjiang. Int.
683 J. Biometeorol. https://doi.org/10.1007/s00484-020-01866-4

684 Kendall MG. 1975. Rank Correlation Methods. Griffin: London.
685 Lee, X., Goulden, M.L., Hollinger, D.Y., Barr, A., Black, T.A., Bohrer, G., Bracho,
686 R., Drake, B., Goldstein, A., Gu, L., Katul, G., Kolb, T., Law, B.E., Margolis,
687 H., Meyers, T., Monson, R., Munger, W., Oren, R., Paw U, K.T., Richardson,
688 A.D., Schmid, H.P., Staebler, R., Wofsy, S., Zhao, L., 2011. Observed increase
689 in local cooling effect of deforestation at higher latitudes. Nature 479, 384–387.
690 https://doi.org/10.1038/nature10588
691 Li, Q., Ma, M., Wu, X., Yang, H., 2018. Snow Cover and Vegetation-Induced
692 Decrease in Global Albedo From 2002 to 2016. J. Geophys. Res. Atmos. 123,
693 124–138. https://doi.org/10.1002/2017JD027010
694 Li, Y., Zhao, M., Motesharrei, S., Mu, Q., Kalnay, E., Li, S., 2015. Local cooling and
695 warming effects of forests based on satellite observations. Nat. Commun. 6.
696 https://doi.org/10.1038/ncomms7603
697 Lu, H., Guan, Y., He, L., Adhikari, H., Pellikka, P., Heiskanen, J., Maeda, E., 2019.
698 Patch aggregation trends of the global climate landscape under future global
699 warming scenario. Int. J. Climatol. https://doi.org/10.1002/joc.6358
700 Mahlstein, I., Daniel, J.S., Solomon, S., 2013. Pace of shifts in climate regions
701 increases with global temperature. Nat. Clim. Chang. 3, 739–743.
702 https://doi.org/10.1038/nclimate1876
703 Mann, H. B. (1945). Nonparametric tests against trend. Econometrica: Journal of the
704 Econometric Society , 245-259.
705 Martin-Benito, D., Pederson, N., 2015. Convergence in drought stress, but a

706 divergence of climatic drivers across a latitudinal gradient in a temperate
707 broadleaf forest. J. Biogeogr. 42, 925–937. https://doi.org/10.1111/jbi.12462
708 McColl, K.A., Alemohammad, S.H., Akbar, R., Konings, A.G., Yueh, S., Entekhabi,
709 D., 2017. The global distribution and dynamics of surface soil moisture. Nat.
710 Geosci. 10, 100–104. https://doi.org/10.1038/ngeo2868
711 Park, S., 2010. IFS Documentation - Cy36r1: PART IV: PHYSICAL PROCESSES
712 1–171.
713 Pauli, H., Gottfried, M., Dullinger, S., Abdaladze, O., Akhalkatsi, M., Alonso, J.L.B.,
714 Coldea, G., Dick, J., Erschbamer, B., Calzado, R.F., Ghosn, D., Holten, J.I.,
715 Kanka, R., Kazakis, G., Kollár, J., Larsson, P., Moiseev, P., Moiseev, D., Molau,
716 U., Mesa, J.M., Nagy, L., Pelino, G., Puşcaş, M., Rossi, G., Stanisci, A.,
717 Syverhuset, A.O., Theurillat, J.P., Tomaselli, M., Unterluggauer, P., Villar, L.,
718 Vittoz, P., Grabherr, G., 2012. Recent plant diversity changes on Europe's
719 mountain summits. Science (80-.). https://doi.org/10.1126/science.1219033
720 Pearson, R.G., Phillips, S.J., Loranty, M.M., Beck, P.S.A., Damoulas, T., Knight, S.J.,
721 Goetz, S.J., 2013. Shifts in Arctic vegetation and associated feedbacks under
722 climate change. Nat. Clim. Chang. 3, 673–677.
723 https://doi.org/10.1038/nclimate1858
724 Peel, M.C., Finlayson, B.L., McMahon, T.A., 2007. Updated world map of the
725 Köppen-Geiger climate classification. Hydrol. Earth Syst. Sci. 11, 1633–1644.
726 https://doi.org/10.5194/hess-11-1633-2007
727 Piao, S., Fang, J., Zhou, L., Guo, Q., Henderson, M., Ji, W., Li, Y., Tao, S., 2003.

728 Interannual variations of monthly and seasonal normalized difference vegetation
729 index (NDVI) in China from 1982 to 1999. J. Geophys. Res. D Atmos. 108, 1–
730 13. https://doi.org/10.1029/2002jd002848
731 Piao, S., Yin, G., Tan, J., Cheng, L., Huang, M., Li, Y., Liu, R., Mao, J., Myneni,
732 R.B., Peng, S., Poulter, B., Shi, X., Xiao, Z., Zeng, N., Zeng, Z., Wang, Y.,
733 2015. Detection and attribution of vegetation greening trend in China over the
734 last 30 years. Glob. Chang. Biol. 21, 1601–1609.
735 https://doi.org/10.1111/gcb.12795
736 Pinzon, J.E., Tucker, C.J., 2014. A non-stationary 1981-2012 AVHRR NDVI3g time
737 series. Remote Sens. 6, 6929–6960. https://doi.org/10.3390/rs6086929
738 Pithan, F., Mauritsen, T., 2014. Arctic amplification dominated by temperature
739 feedbacks in contemporary climate models. Nat. Geosci. 7, 181–184.
740 https://doi.org/10.1038/ngeo2071
741 Ren, Z., Zhang, M., Wang, S., Qiang, F., Zhu, X., Dong, L., 2015. Changes in daily
742 extreme precipitation events in South China from 1961 to 2011. J. Geogr. Sci.
743 25, 58–68. https://doi.org/10.1007/s11442-015-1153-3
744 Richardson, A.D., Keenan, T.F., Migliavacca, M., Ryu, Y., Sonnentag, O., Toomey,
745 M., 2013. Climate change, phenology, and phenological control of vegetation
746 feedbacks to the climate system. Agric. For. Meteorol. 169, 156–173.
747 https://doi.org/10.1016/J.AGRFORMET.2012.09.012
748 Rohli, R. V., Andrew Joyner, T., Reynolds, S.J., Shaw, C., Vázquez, J.R., 2015a.
749 Globally Extended Kppen-Geiger climate classification and temporal shifts in

terrestrial climatic types. Phys. Geogr. 36, 142–157. https://doi.org/10.1080/02723646.2015.1016382

Rohli, R. V., Joyner, T.A., Reynolds, S.J., Ballinger, T.J., 2015b. Overlap of global Köppen–Geiger climates, biomes, and soil orders. Phys. Geogr. 36, 158–175. https://doi.org/10.1080/02723646.2015.1016384

Rubel, F., Kottek, M., 2010. Observed and projected climate shifts 1901-2100 depicted by world maps of the Köppen-Geiger climate classification. Meteorol. Zeitschrift 19, 135–141. https://doi.org/10.1127/0941-2948/2010/0430

Schaaf, C.B., Gao, F., Strahler, A.H., Lucht, W., Li, X., Tsang, T., Strugnell, N.C., Zhang, X., Jin, Y., Muller, J., Lewis, P., Barnsley, M., Hobson, P., Disney, M., Roberts, G., Dunderdale, M., Doll, C., Robert, P., Hu, B., Liang, S., Privette, J.L., Roy, D., 2002. First operational BRDF, albedo nadir reflectance products from MODIS 83, 135–148.

Scheffer, M., Carpenter, S., Foley, J.A., Folke, C., Walker, B., 2001. Catastrophic shifts in ecosystems. Nature 413, 591–596. https://doi.org/10.1038/35098000

Shen, M., Piao, S., Jeong, S.-J., Zhou, L., Zeng, Z., Ciais, P., Chen, D., Huang, M., Jin, C.-S., Li, L.Z.X., Li, Y., Myneni, R.B., Yang, K., Zhang, G., Zhang, Y., Yao, T., 2015. Evaporative cooling over the Tibetan Plateau induced by vegetation growth. Proc. Natl. Acad. Sci. 112, 9299–9304. https://doi.org/10.1073/pnas.1504418112

Stark, S.C., Breshears, D.D., Garcia, E.S., Law, D.J., Minor, D.M., Saleska, S.R., Swann, A.L.S., Villegas, J.C., Aragão, L.E.O.C., Bella, E.M., Borma, L.S.,

772 Cobb, N.S., Litvak, M.E., Magnusson, W.E., Morton, J.M., Redmond, M.D.,
773 2016. Toward accounting for ecoclimate teleconnections: intra- and inter-
774 continental consequences of altered energy balance after vegetation change.
775 Landsc. Ecol. 31, 181–194. https://doi.org/10.1007/s10980-015-0282-5
776 Sunday, J.M., Bates, A.E., Dulvy, N.K., 2011. Global analysis of thermal tolerance
777 and latitude in ectotherms. Proc. R. Soc. B Biol. Sci. 278, 1823–1830.
778 https://doi.org/10.1098/rspb.2010.1295
779 Tucker, C.J., Pinzon, J.E., Brown, M.E., Slayback, D.A., Pak, E.W., Mahoney, R.,
780 Vermote, E.F., El Saleous, N., 2005. An extended AVHRR 8-km NDVI dataset
781 compatible with MODIS and SPOT vegetation NDVI data. Int. J. Remote Sens.
782 26, 4485–4498. https://doi.org/10.1080/01431160500168686
783 Turco, M., Von Hardenberg, J., AghaKouchak, A., Llasat, M.C., Provenzale, A.,
784 Trigo, R.M., 2017. On the key role of droughts in the dynamics of summer fires
785 in Mediterranean Europe. Sci. Rep. 7, 1–10. https://doi.org/10.1038/s41598-017-
786 00116-9
787 Wang, M., Overland, J.E., 2004. Detecting arctic climate change using Köppen
788 climate classification. Clim. Change 67, 43–62. https://doi.org/10.1007/s10584-
789 004-4786-2
790 Williams, J.W., Jackson, S.T., Kutzbach, J.E., 2007. Projected distributions of novel
791 and disappearing climates by 2100 AD. Proc. Natl. Acad. Sci. U. S. A. 104,
792 5738–5742. https://doi.org/10.1073/pnas.0606292104
793 Wu, D., Zhao, X., Liang, S., Zhou, T., Huang, K., Tang, B., Zhao, W., 2015. Time-lag

794 effects of global vegetation responses to climate change. Glob. Chang. Biol. 21,
795 3520–3531. https://doi.org/10.1111/gcb.12945
796 Wu, J., 2004. Effects of changing scale on landscape pattern analysis: Scaling
797 relations. Landsc. Ecol. 19, 125–138.
798 https://doi.org/10.1023/B:LAND.0000021711.40074.ae
799 Yang, Y., Roderick, M.L., Zhang, S., McVicar, T.R., Donohue, R.J., 2018.
800 Hydrologic implications of vegetation response to elevated CO2 in climate
801 projections. Nat. Clim. Chang. https://doi.org/10.1038/s41558-018-0361-0
802 Zhao, Y., 2018. Vegetation and climate reconstructions on different time scales in
803 China: a review of Chinese palynological research. Veg. Hist. Archaeobot. 27,
804 381–392. https://doi.org/10.1007/s00334-017-0655-6
805 Zhao, Y., Herzschuh, U., Li, Q., 2015. Complex vegetation responses to climate
806 change on the Tibetan Plateau: A paleoecological perspective. Natl. Sci. Rev. 2,
807 400–402. https://doi.org/10.1093/nsr/nwv057
808 Zhu, X., Li, Y., Li, M., Pan, Y., Shi, P., 2013. Agricultural irrigation in China. J. Soil
809 Water Conserv. 68, 147–154. https://doi.org/10.2489/jswc.68.6.147A
810
811 **Figure 1.** Distribution of (a) annual average temperature (China's ground temperature
812 0.5° × 0.5° grid dataset) (http://data.cma.cn/data/index/), (b) annual average
813 precipitation (China's ground precipitation 0.5° × 0.5° grid dataset), (c) topography

(SRTM DEM) (http://www.gscloud.cn/), and (d) vegetation types extracted from year 2000 land cover data (http://www.resdc.cn/) in China.

Figure 2. Trends in (a) annual average temperature and (b) precipitation and correlations of NDVI to (c) temperature and (d) precipitation during 1982–2012.

Figure 3. The spatial distribution of the Köppen climate zones in China for (a) 1982, (b) 1990, (c) 2000, and (d) 2010. Each year represents an average period of five consecutive years. A–E represents tropical, arid, temperate, continental, and alpine climates, respectively. During 1990–2000, shifts between continental and arid climates predominantly occurred in the Northeast Plain.

Figure 4. Cumulative percentage of area change of all climate zones in China during 1983–2012. The temporal trend was statistically significant at the significance level of 0.05, based on the MK test.

Figure 5. Temporal variations of percentage area for (a) arid, (b) temperate, (c) continental, and (d) alpine zones in China during 1982–2012. Changes in climatic type percentage areas are based on 5-yr running means of ground temperature and precipitation 0.5° × 0.5° grid datasets. Note that the y-axis scale differs between climatic zones.

Figure 6. Sensitivity analysis of (a) arid, (b) temperate, (c) continental, and (d) alpine zones. S_{precip} and S_{temp} represent the sensitivity analysis results with precipitation or temperature held constant, respectively. The results show that precipitation is the dominant driver in the arid and continental climate zones, while temperature is the dominant driver in the temperate and alpine climate zones. All fittings were

836 statistically significant ($p < 0.01$, t-test). Note that the axis scale differs between
837 climatic zones.
838 **Figure 7.** Trends in (a) surface SW content (ERA-interim), (b) NDVI (GIMMS), (c)
839 albedo (ERA-interim), and (d) the correlation between albedo and NDVI from 1982
840 to 2012. Statistically significant correlations ($p < 0.05$) are marked with crosses.
841 **Figure 8.** The response of the percentage area (PA) to its dominant climate control
842 (temperature or precipitation) in (a) arid, (b) temperate, (c) continental, and (d) alpine
843 climate zones from 1982 to 2012. The percentage area is indicated by the location of
844 circles, while mean NDVI is indicated by the colour of the circles. Changes in
845 percentage area are negatively correlated to precipitation in arid climate and to
846 temperature in alpine climate, while percentage area change is positively correlated to
847 temperature in temperate climate and to precipitation in continental climate. The
848 histograms indicate changes in the surface SW anomaly.
849 **Figure 9.** The relationship between annual NDVI (red lines) and albedo (blue line)
850 from 1982 to 2012.
851 **Figure 10.** Monthly trends in NDVI, albedo, and SW anomaly for (a) arid, (b)
852 temperate, (c) continental, and (d) alpine climate zone during 1982–2012. The green
853 shaded areas represent the growing period (Arid: May to October; Temperate: April to
854 November; Continental: May to mid-October; Alpine: May to mid-September). The
855 clear monthly trends in NDVI, albedo, and SW content occur during the growing

856 period. The temporal trend was statistically significant at the significance level of
857 0.05, based on the MK test.

858 **Table 1.** Remote sensing and meteorological reanalysis dataset characteristics

859 **Table 2.** Changes in percentage area of different periods relative to baseline time
860 (1982).

861 **Table 3.** Qualitative sensitivity parameters of the percentage area in each climate
862 zone where either temperature or precipitation is held constant.

Tables

Table 1. Remote sensing and meteorological reanalysis dataset characteristics

Data type	Product	Version	Spatial resolution	Temporal resolution	Timestep
NDVI	GIMSS NDVI3g	V0	0.0833° × 0.0833°	Half month	1982–2012
Temperature	China's ground temperature 0.5° × 0.5° Grid data set	V2.0	0.5° × 0.5°	Monthly	1982–2012
Precipitation	China's ground precipitation 0.5° × 0.5° Grid data set	V2.0	0.5° × 0.5°	Monthly	1982–2012
Albedo	ERA-Interim	V2.0	0.125° × 0.125°	Monthly	1982–2012
Volumetric soil water	ERA-Interim	V2.0	0.125° × 0.125°	Monthly	1982–2012
Topography	SRTM DEM	\	1 km	\	2000
Vegetation type	Land use/cover (2000)	\	1 km	\	2000

Table 2. Changes in percentage area of different periods relative to baseline time (1982).

Comparison	Arid	Temperate	Continental	Alpine
ΔPA_{1990}	–1.10	1.34	0.20	–0.47
ΔPA_{2000}	3.01	0.95	–3.72	–0.33
ΔPA_{2010}	–1.74	0.24	1.95	–0.50

Table 3. Qualitative sensitivity parameters of the percentage area in each climate zone where either temperature or precipitation is held constant.

Zones	Sensitivity parameter	Linear regression equation	Coefficients of determination (r^2)	Significance (p)
B	**S_{precip}**	**y = 0.74x + 7.73**	**0.856**	***p* < 0.01**
	S_{temp}	y = 0.3x + 19.58	0.473	$p < 0.01$
C	S_{precip}	y = 0.13x + 20.18	0.646	$p < 0.01$
	S_{temp}	**y = 0.95x + 1.39**	**0.980**	***p* < 0.01**
D	**S_{precip}**	**y = 0.59x + 11.12**	**0.815**	***p* < 0.01**
	S_{temp}	y = 0.49x + 17.21	0.753	$p < 0.01$
E	S_{precip}	y = –1.31x + 40.57	0.514	$p < 0.01$
	S_{temp}	**y = 1.28x – 5.47**	**0.968**	***p* < 0.01**

B–E represent arid, temperate, continental, and alpine climates, respectively.

Figure 1. Distribution of (a) annual average temperature (China's ground temperature 0.5° × 0.5° grid dataset) (http://data.cma.cn/data/index/), (b) annual average precipitation (China's ground precipitation 0.5° × 0.5° grid dataset), (c) topography (SRTM DEM) (http://www.gscloud.cn/), and (d) vegetation types extracted from year 2000 land cover data (http://www.resdc.cn/) in China.

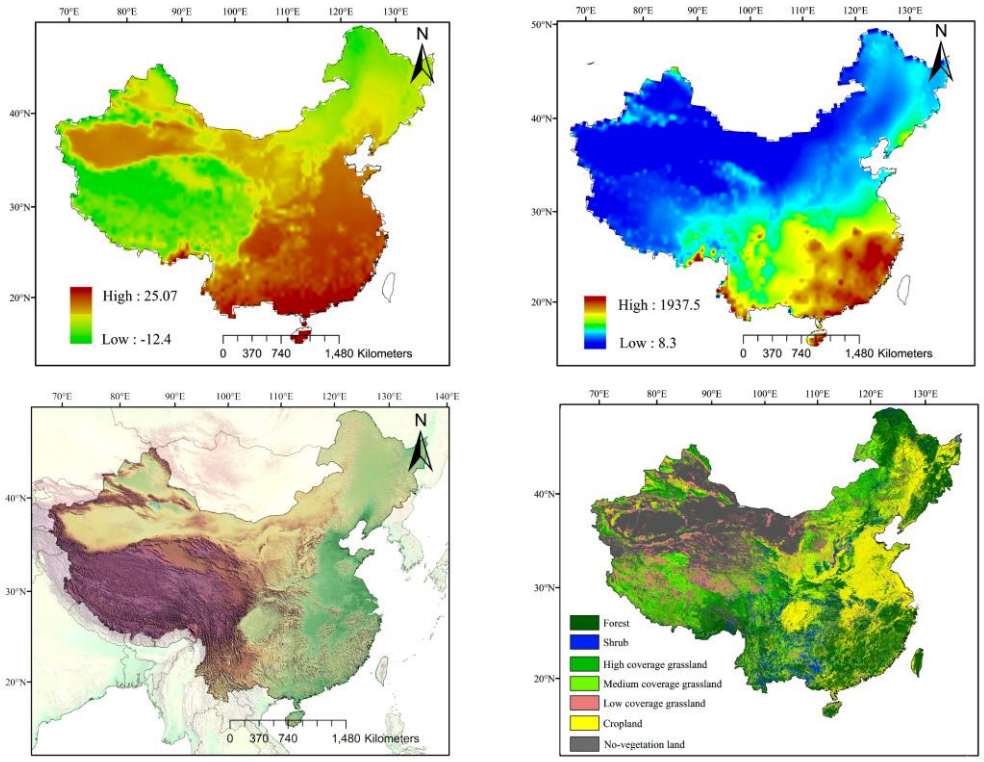

Figure 2. Trends in (a) annual average temperature and (b) precipitation and correlations of NDVI to (c) temperature and (d) precipitation during 1982–2012.

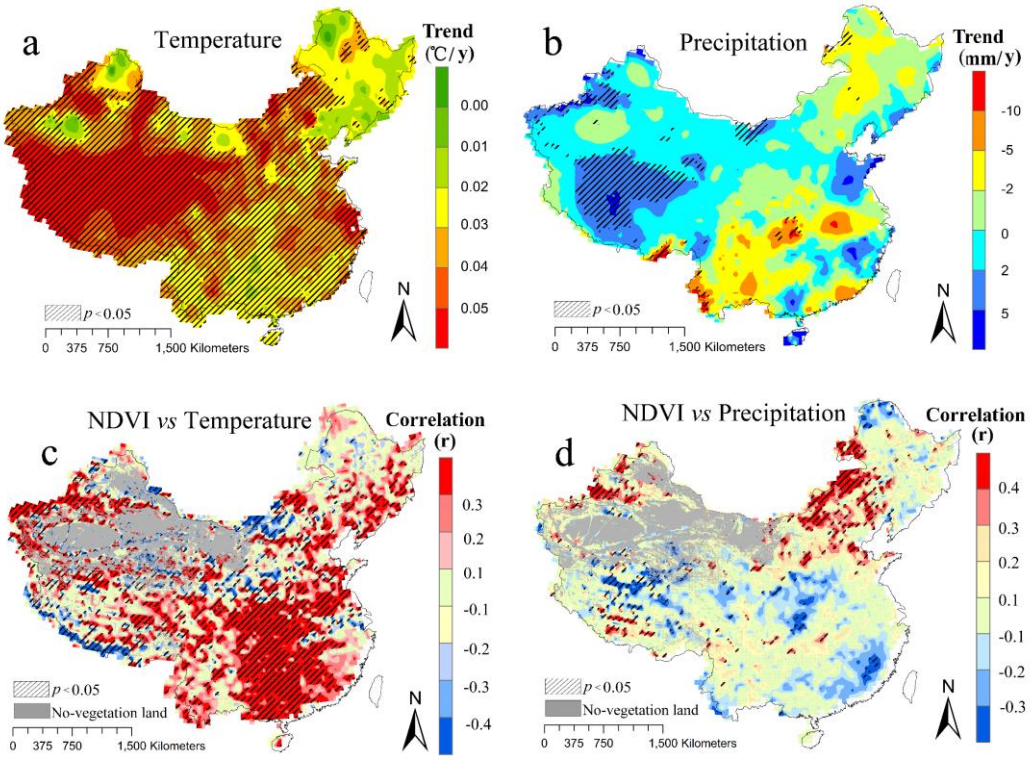

Figure 3. The spatial distribution of the Köppen climate zones in China for (a) 1982, (b) 1990, (c) 2000, and (d) 2010. Each year represents an average period of five consecutive years. A–E represents tropical, arid, temperate, continental, and alpine climates, respectively. During 1990–2000, shifts between continental and arid climates predominantly occurred in the Northeast Plain.

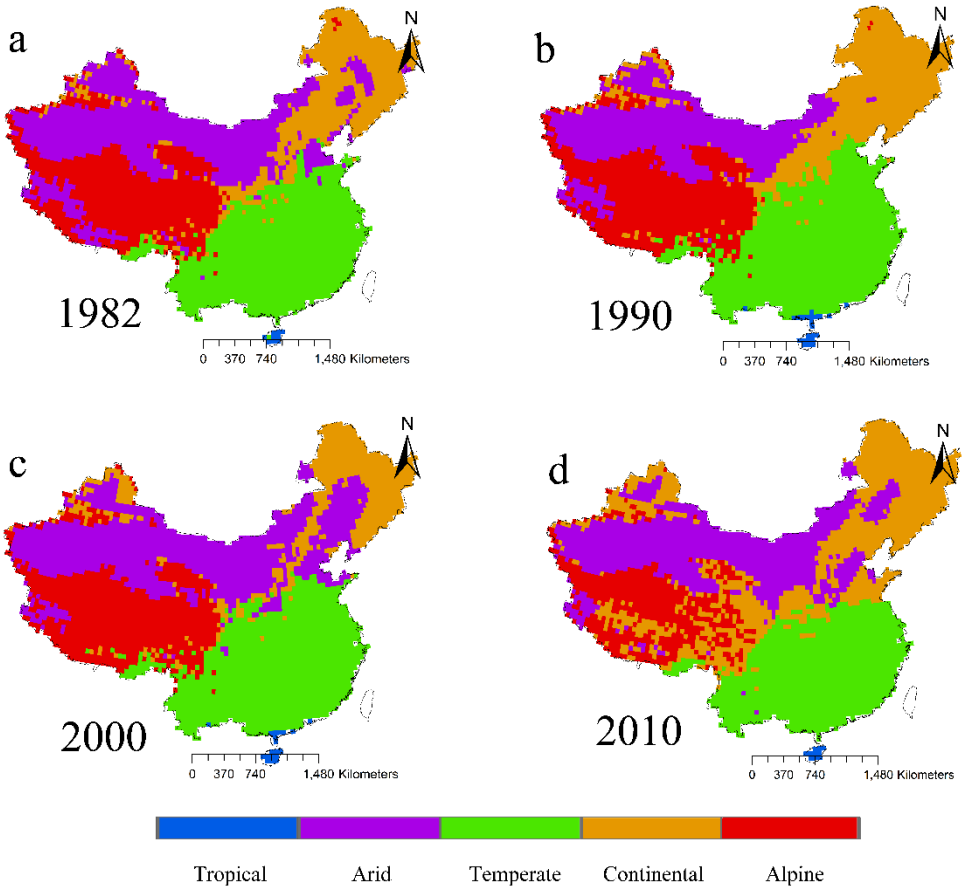

Figure 4. Cumulative percentage of area change of all climate zones in China during 1983–2012. The temporal trend was statistically significant at the significance level of 0.05, based on the MK test.

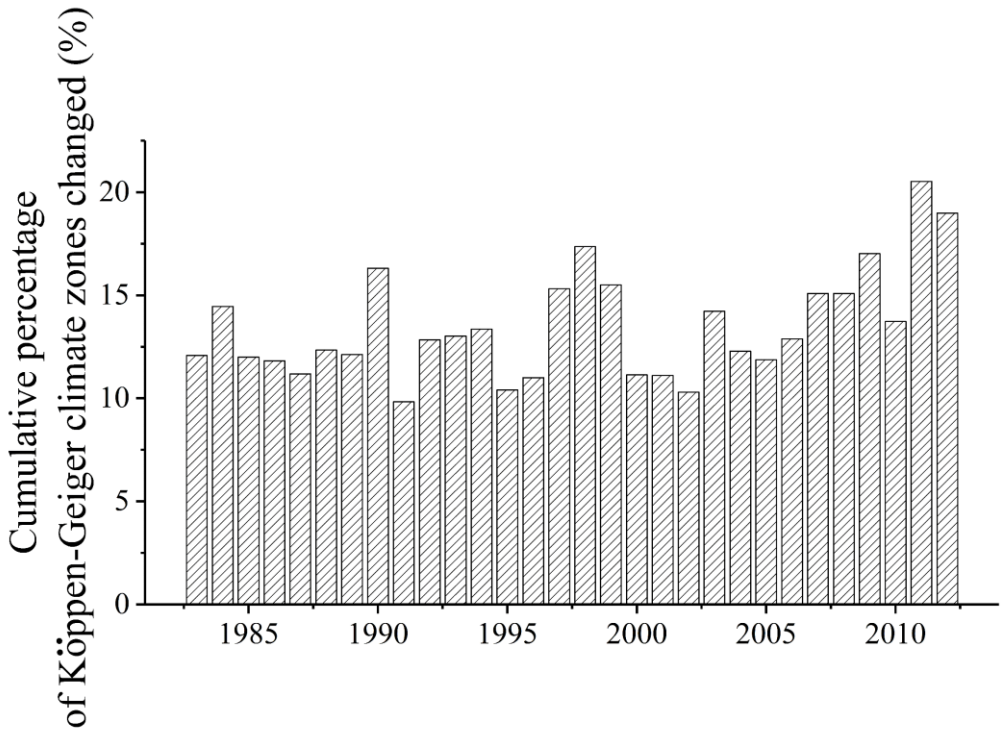

Figure 5. Temporal variations of percentage area for (a) arid, (b) temperate, (c) continental, and (d) alpine zones in China during 1982–2012. Changes in climatic type percentage areas are based on 5-yr running means of ground temperature and precipitation 0.5° × 0.5° grid datasets. Note that the y-axis scale differs between climatic zones.

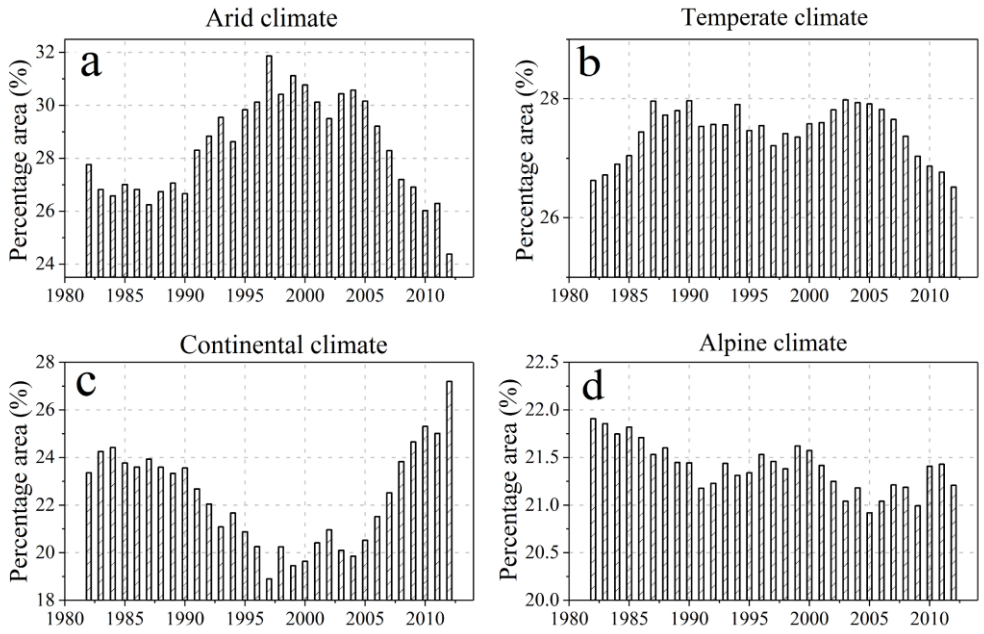

Figure 6. Sensitivity analysis of (a) arid, (b) temperate, (c) continental, and (d) alpine zones. S_{precip} and S_{temp} represent the sensitivity analysis results with precipitation or temperature held constant, respectively. The results show that precipitation is the dominant driver in the arid and continental climate zones, while temperature is the dominant driver in the temperate and alpine climate zones. All fittings were statistically significant ($p < 0.01$, t-test). Note that the axis scale differs between climatic zones.

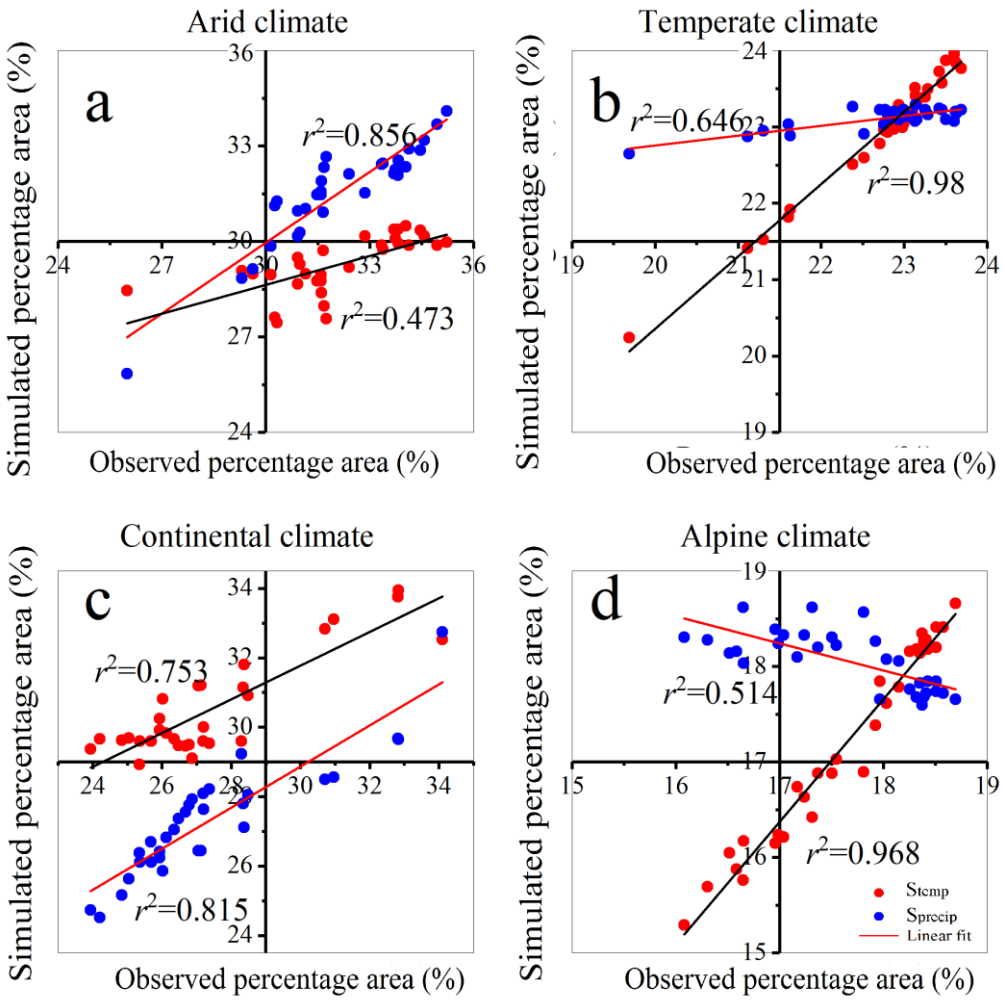

Figure 7. Trends in (a) surface SW content (ERA-interim), (b) NDVI (GIMMS), (c) albedo (ERA-interim), and (d) the correlation between albedo and NDVI from 1982 to 2012. Statistically significant correlations ($p < 0.05$) are marked with crosses.

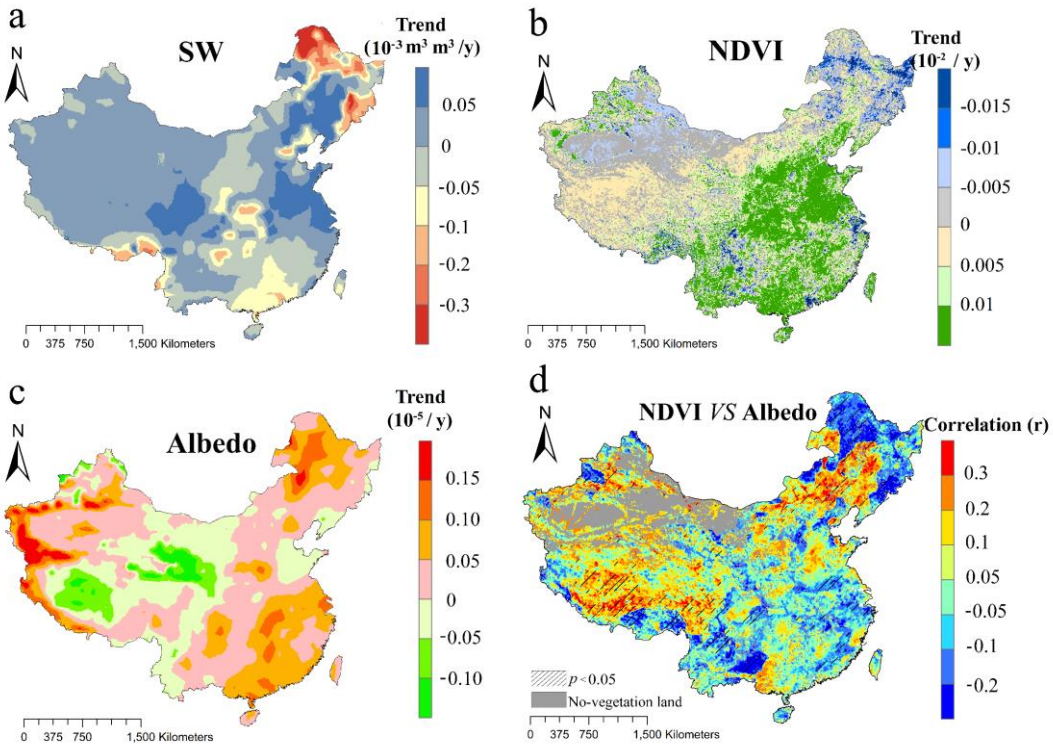

Figure 8. The response of the percentage area (PA) to its dominant climate control (temperature or precipitation) in (a) arid, (b) temperate, (c) continental, and (d) alpine climate zones from 1982 to 2012. The percentage area is indicated by the location of circles, while mean NDVI is indicated by the colour of the circles. Changes in percentage area are negatively correlated to precipitation in arid climate and to temperature in alpine climate, while percentage area change is positively correlated to temperature in temperate climate and to precipitation in continental climate. The histograms indicate changes in the surface SW anomaly.

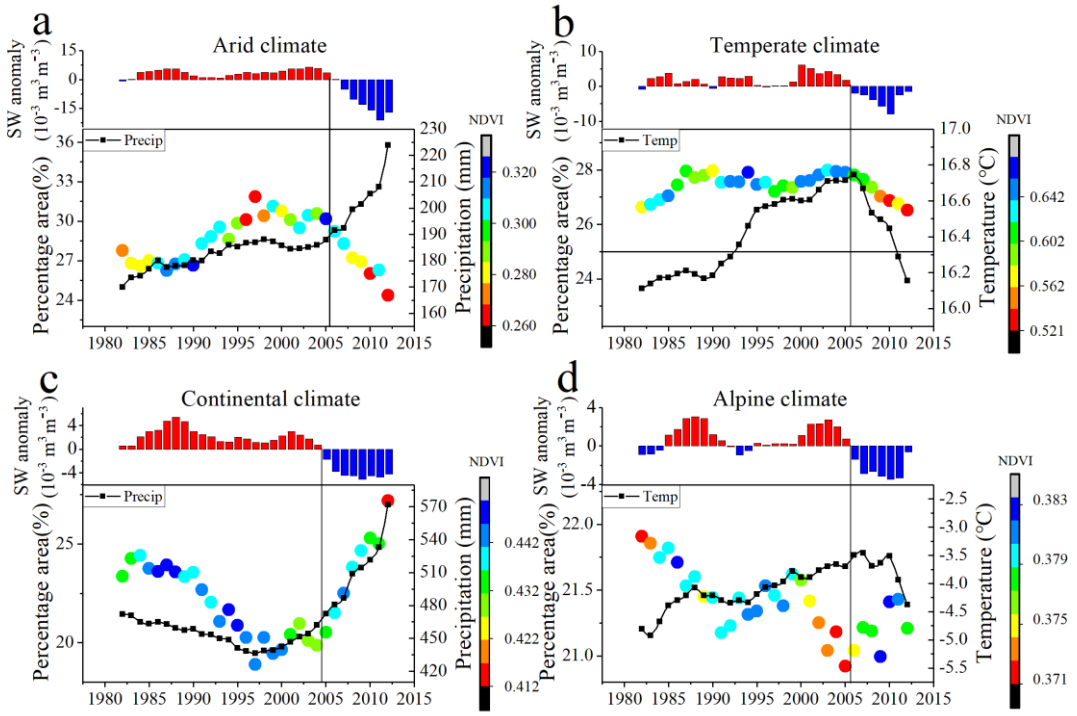

Figure 9. The relationship between annual NDVI (red lines) and albedo (blue line) from 1982 to 2012.

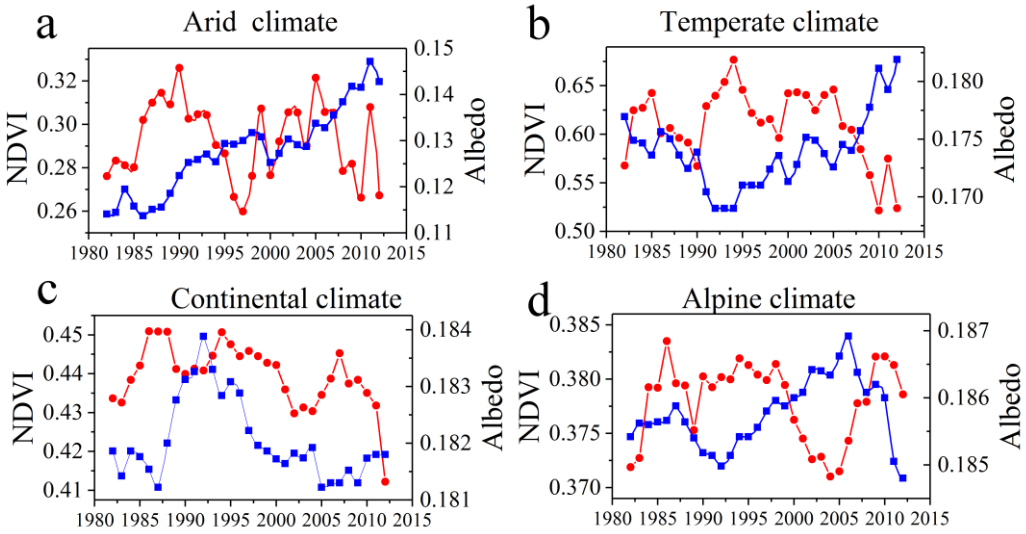

Figure 10. Monthly trends in NDVI, albedo, and SW anomaly for (a) arid, (b) temperate, (c) continental, and (d) alpine climate zone during 1982–2012. The green shaded areas represent the growing period (Arid: May to October; Temperate: April to November; Continental: May to mid-October; Alpine: May to mid-September). The clear monthly trends in NDVI, albedo, and SW content occur during the growing period. The temporal trend was statistically significant at the significance level of 0.05, based on the MK test.